Energy Conversion and Management 288 (2023) 117101

Contents lists available at ScienceDirect

Energy Conversion and Management

journal homepage: www.elsevier.com/locate/enconman

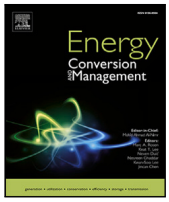

Concept design and energy balance optimization of a hydrogen fuel cell helicopter for unmanned aerial vehicle and aerotaxi applications

A. Tiseira, R. Novella, L.M. Garcia-Cuevas, M. Lopez-Juarez *

CMT-Motores Térmicos, Universitat Politècnica de València, Camino de vera s/n, 46022 Valencia, Spain

ARTICLE INFO

Keywords:
Hydrogen fuel cell
Helicopter
Energy balance optimization
UAV
Aerotaxi
Aerodynamic design

ABSTRACT

In the new scenario where the transportation sector must be decarbonized to limit global warming, fuel cell-powered aerial vehicles have been selected as a strategic target application to compose part of the urban fleet to minimize road transport congestion and make goods and personal transportation fast and efficient. To address the necessity of clean and efficient urban air transport, this work consists of the conceptual development of a lightweight rotary-winged transport vehicle using a hydrogen-based fuel cell propulsion system and the optimization of its energy balance. For that purpose, the methods for integrating the coupled aerodynamic and propulsion system sizing and optimization was developed with the aim of designing concepts capable of carrying 0 (unmanned aerial vehicle — Design 1) and 1 (Aerotaxi — Design 2) passengers for a distance of 300 km at a cruise altitude of 500 m with a minimum climbing rate capability of 6 m s^{-1} at 1000 m. The results show how these designs with the desired performance specifications can be obtained with a vehicle mass ranging from 416 to 648 kg, depending on the application, and with specific range and endurance respectively within 46.2–47.8 km/kg and 20.4–21.3 min/kg for design 1 and 33.3–33.8 km/kg and 12.5–13.9 min/kg for design 2.

1. Introduction

Today, sustainability has to be considered in all areas of industry, and aviation and transport are no exception. Now, after a turning point caused by the COVID-19 pandemic, the World is slowly returning to its normal habit of personal travel. The rise of new technologies applied to the development of new propulsion methods is leading to compatibility in the use of transport and the environment. The number of passengers by air, land or sea is expected to increase considerably in the last quarter of 2022, close to the values of 2019 [1]. Therefore, it is important to implement sustainable transport systems. In air transport vehicles, sustainability lies in five main aspects: aerodynamics, propulsion, production, maintenance and navigation. This work focuses on the propulsive aspect involving a rotary wing aircraft that can be employed for various missions. The chosen aircraft is located in the light helicopter segment and the study is based on the implementation of a sustainable propulsion system. This segment of aircraft has undergone a powerful development since its inclusion in the 1990s as recreational aircraft or for transport by private users, commonly using an internal combustion engine (ICE). Now, this class of helicopters is being designed for different missions such as surveillance, passenger transport, various aerial works, etc [2]. In addition, there are different piloting versions according to the mission, making the aircraft autonomous or commanded.

According to the European Union Aviation Safety Agency (EASA), very light rotorcraft (VLR) have a maximum certified take-off mass lower than 600 kg [3]. They tend to have good maneuverability and are agile enough to fly over difficult terrains due to their size in relation to the installed power. These qualities have made it possible for this type of aircraft to be used as a means of urban transport in large cities, connecting nerve centers with interurban or international transport zones such as ports, airports and high-speed, long-distance train stations.

The mission of the rotorcraft studied in this paper is that of a short-range, short-endurance, inter-zonal air taxi with the capacity to transport two or three passengers. The aircraft is expected to fly completely autonomously, without a pilot. In addition, it is also designed for passenger-less, forest surveillance platforms. The power requirement for this aircraft segment does not exceed 120 kW, many of which are around 84 kW, as it is shown in Table A.6. The powerplant in VLR is usually a petrol or, rarely, diesel engine with turbocharger and gearbox on the main rotor and anti-torque tail rotor. These type of engines are widely used in the automotive industry, and is currently facing

* Corresponding author.
E-mail address: marlojua@mot.upv.es (M. Lopez-Juarez).
URL: http://www.cmt.upv.es (M. Lopez-Juarez).

https://doi.org/10.1016/j.enconman.2023.117101
Received 12 December 2022; Received in revised form 17 April 2023; Accepted 21 April 2023
Available online 11 May 2023

challenging difficulties in overcoming the required limits of pollutant and greenhouse gas emissions (CO_2, NO_x, soot, etc.). Meanwhile, the European Union's strategy to become climate neutral by 2050 includes air transport [4], so new developments such as the aircraft studied in this paper are expected to produce no net greenhouse gas emissions in less than 30 years. Therefore, the powerplant for the urban mission of the conceptual aircraft must be battery-electric, powered by a fuel cell (FC), hydrogen-burning ICE or a hybrid of these options [5]. In any case, different roadmaps, be them specific to aviation [6] or to all the sectors [7], coincide that the actual decrease in emissions would only be achievable if the H_2 is green, i.e., it is produced from renewable energy sources. The battery-electric option, although relatively simple and attractive for lower mass, very low range and endurance applications, usually leads to prohibitive battery masses and volumes when transporting passengers with VLR. Although batteries with better resistance to thermal runaway issues [8], faster charging, higher specific energy and energy density and higher power density batteries are being actively researched right now, this paper focuses on a hybrid system that uses the batteries only as an energy buffer for peak demand. Regarding hydrogen ICEs, although they have some durability advantages against FCs, are discarded due to their lower efficiencies.

Following this line of thought, the scientific community has invested significant effort into developing FC technology for transport applications. Applied studies are mostly focused on the sizing of the fuel cell system (FCS), the battery, and the H_2 tank for transport applications such as light-duty passenger cars to quantify their performance [9] and environmental impact [10], both integrating the effect of the FCS dynamics [11] or component size [12] on FC degradation, or even the vehicle body or curb weight [13]. These studies are mostly focused on but are not limited to, road transport applications with semi-empirical FC degradation models [14]. In this sense, it is also possible to find sizing analyses for railway [15] or maritime [16] transport applications. For aerospace vehicles, the studies integrating FC technology into the propulsion systems are limited and further research is required. In this sense, there are two main research currents in the aerospace sector. On one hand, there are studies that aim at understanding the feasibility of integrating the FC technology (solid-oxide, mainly) as a substitute for the turbine to power the compressor in a jet engine [17]. On the other hand, some researchers aim at integrating low-temperature FC-based propulsion systems in small unmanned aerial vehicles (UAV) for different types of missions, such as long-endurance ones [18]. More authors are publishing encouraging results for low-temperature FC-based propulsion systems in UAVs, such as Ozbek et al. [19], who experimentally measured the power consumption of a fixed-wing UAV during flight, designed an hybrid powertrain and proceded to ground test it. Some authors are even performing life cycle assessments: Çalışır et al. [20] found important reductions in global warming potential, terrestrial ecotoxicity and photochemical oxidation. For rotorcraft, however, the published material is more limited. As far as the authors of this manuscript know, the most advanced available work about models of FC systems for very light rotorcraft that may be used for conceptual design was published by Datta and Johnson [21] in 2014: the authors presented a complete model of the fuel cell system, including the losses of the balance of plant as a function of the flight altitude, and performed a comprehensive analysis of the performance of the system for a two-seat Robinson R22 Beta II helicopter. The model presented in their work, however, may be somewhat limited when computing complex missions, as some of the assumptions are not completely valid in a wide operating range of conditions. Such is the case of the compressor–expander, which are modeled with a constant efficiency independent of the operating point. Finally, from an experimental point of view, although it is possible to find detailed analysis of low-temperature fuel cell systems for small UAVs and comparisons against manufacturer's data, such as in the work by Santos et al. [22], it is not possible to find detailed results for altitude operation, at least in the 50–100 kW range.

Given the lack of research in this field, this study aims at proving the feasibility of integrating a FC-based propulsion system into a helicopter vehicle for UAV and aerotaxi applications by sizing the FCS and optimizing its energy balance at different altitudes. The FCS model used for the design includes the influence of several working parameters not included in other works, so its sizing is expected to be much more adjusted to reality.

1.1. Knowledge gaps

In the progress to improve the quality of life and reduce pollutants in cities, transport systems must be zero-emission. Urban air transport is part of the future and must be driven by a sustainable system. Fuel cells are an option but their inclusion in the air vehicle must be studied in relation to the performance offered by the propulsion plant that must move the main rotor and tail rotor. None of the studies found in the literature identify the size of the components in the FC-based propulsion system for the light-weight helicopter application be it a UAV or an air taxi. Furthermore, there is not a clear understanding of the specific endurance and range of these vehicles combined with zero-emissions propulsion systems. This is mainly due to the added difficulty of coupling the sizing of the propulsion system components to the aerodynamic design, namely the H_2 tanks, defined by the vehicle target mission.

1.2. Objectives and motivation

The motivation of this study is mainly to provide the scientific community and the industry with a conceptual design of a light helicopter with a hydrogen-based fuel cell engine. This is novel in itself since there is limited data about the design of the propulsion system that makes this concept feasible. As a key point of this study the FCS efficiency was optimized for each altitude with an altitude-aware air management strategy, thus obtaining the optimum evolution of the FCS net power output capacity with altitude, which is critical to make the sizing of the helicopter compatible. Furthermore, given the high mass and volume of modern H_2 storage systems, the calculation of the storage volume is important to define the aerodynamics of the aircraft. It is important to note that part of sustainability is related to aerodynamics and aerodynamics is related to the energy consumption of the engine implemented in the flying vehicle. In addition, the system can be under control where the stability of the aircraft can be simplified by means of two batteries each coupled to a rotor. The decoupled system lightens the operational empty mass (OEM) of the aircraft. Therefore, it is necessary to address the feasibility of this system and how the power distribution is.

Therefore, this study is intended to constitute a guideline for preliminary sizing for FC-powered light helicopters considering detailed aspects such as the penalty on FCS efficiency with altitude, the aerodynamic implications of integrating the H_2 tanks into the vehicle and the decoupled e-motor system performance.

The general objective of this work is to demonstrate, by means of a conceptual study, the use of a fuel cell to power a very light rotorcraft to be used as an air taxi or UAV. The following particular milestones can be highlighted in the work:

- Conceptual design of a helicopter with a propulsion system based on fuel cell technology with a maximum range of $300\,\mathrm{km}$ at cruise altitude ($500\,\mathrm{m}$), capable of climbing at a rate of $6\,\mathrm{m\,s^{-1}}$ at an altitude of $1000\,\mathrm{m}$. Two designs are considered: an UAV application (design 1 - 0 passengers) and air taxi application (design 2 - 1 passenger).
- Adaptation of the 1-passenger design to carry 2 passengers.
- Study of the behavior of the fuel cell at different altitudes and optimization of the balance of plant management to ensure the maximum efficiency at each combination of current density and altitude.

- Optimization of the required mass of fuel in the tank and mission: identification of the range and endurance capabilities of the selected designs and possible variations.
- Identification of the dimensions and location of the hydrogen tanks in the helicopter.

2. Methods on the aerodynamic design and integration

The conceptual design used in this work into account the dimensions and weight distribution of the individual components of the aircraft, including the fuel cell. The various parameters used in the design phase are obtained from correlations fitted to data from other rotary-wing vehicles with similar characteristics. The selected helicopters have a maximum take-off mass (MTOM) range between 450 and 780 kg. A total of 9 helicopters have been selected as a basis for obtaining information on geometry, weights and components. The data can be found in Appendix A. The center of mass calculation as well as the transmission components have been developed using the descriptions found in the literature, as in the Helicopter Flying Handbook by the Federal Aviation Administration [23] or the work of Astridge about Helicopter Transmissions — design [24]. The fundamental components are described in these works. The transmission is adapted to the use of the fuel cell for both the main rotor and the anti-torque. The weights estimation has been calculated using the equations proposed by Prouty [25]. The weights of the hydrogen tanks and the fuel cell systems were obtained from the existing standard technological data. The weight and placement of the different elements that make up a helicopter depend on many factors such as its mission, the number of engines, etc. The placement of these elements cannot be random as the basic elements of a helicopter (rotors, engines, transmission, etc.) must be cohesive in continuous interaction with each other. Therefore, the helicopter balance is a critical section in the conceptual design of a helicopter, where it is said that a deviation of 8 cm from the center of gravity in a helicopter with maximum load can lead to the undesired behavior of the aircraft [26].

The helicopter parameters presented in this paper are based on data from existing helicopters in the same segment. The number chosen was 9. Table 1 gives some of the parameters used to size the helicopter to operate with a fuel cell and a battery to assist in take-off. The mass range is between 450 to 780 kg among the chosen helicopters.

Furthermore, as can be seen in the table, three versions of the device have been made taking into account different factors. One of them is the transport configuration with one or two people, that means pilot or pilot plus passenger because the configuration in terms of avionics and instrumental configuration change respect the UAV design. Therefore, in the first case with one person, this configuration has a take-off mass close to 608 kg, while for two people as pilot and passenger has a value of around 648 kg with reduced additional payload (15 kg). To achieve this value the 2 P version has no extra payload weight and has a H_2 tank mass close to 15 kg as opposed to 45 kg for a single passenger version (1 P). The range of the second version is significantly reduced because the H_2 storage is smaller. However, this version can be useful for a shuttle mission between neuralgic points in large cities, serving as an air taxi. In cities such as NY, Paris etc., a study shows that the use of sustainable air mobility will be limited to a range of 24 to 32 km per trip in a relatively short time [27].

The helicopter sizing criterion responds to the mission and the segment chosen to be represented according to its weight and power. In this work, the following observations have been taken into account with respect to an autonomy according to the requirements of each of the versions of the helicopter with 1, 2 passengers and in its UAV version, as well as the range. Therefore, calculations have been made according to a cruising speed based on the data obtained from the values of similar helicopters belonging to the same segment and the payload has been adjusted depending on the choice of the mission with reference to the three configurations detailed in Table 1. Finally, the service ceiling has been defined in relation to the main mission of transporting people by a sustainable aerial means, set at 500 m, but it is possible for the engine to reach 1000 m. In this work, the main theoretical study lies in adjusting the power delivered by the battery to reach the altitude at which the device must fly, as well as the adequate power required to adjust the ascent to the altitude demand and the energy demand of the battery to be able to deliver the power required to reach the altitude.

Table 1
Helicopter mass segmentation for design 1 and design 2 with 1 and 2 passengers. The mass segmentation for UAV application of design 2 is that described for 1 passenger without the weight associated to passengers.

Component	Mass [kg] Design 1 (UAV)	Mass [kg] Design 2 (1P)	Mass [kg] Design 2 (2P)
Fuel cell	123	184	184
Main engine	43	61.2	61.2
Tail engine	2.2	3	3
Battery [2 kWh]	9	9	9
H_2 tanks	32,5	45	15
Fuselage	63.4	73	73
Main rotor	70	71.5	71.5
Tail rotor	1.8	1.8	1.8
Tail structure	6.4	6.4	6.4
Landing gear	6.5	6.5	6.5
Hydraulics	12	14	14
Avionics	5	5	5
Power electronics	7.5	7.5	7.5
Equipment	2.5	4	4
Instrumentation	1.5	3	3
Cabin controls	5.2	12	12
Rear structure	6.5	6.5	6.5
Passengers	0	75	150
Additional payload	18	20	15
Total	416	608	648

2.1. Power required for cruise

The vehicle has been calculated for different cruise flight conditions. Each of the configurations has a different speed. Table 2 shows how the cruise speed is modified depending on the altitude, the weight of the helicopter and the power that the main rotor must have. Each speed value is related to the maximum possible range that the vehicle can have at each cruising altitude value. For this work, it has been decided that the design altitude is 500 m because most of the helicopters in this segment operate at this altitude. Table 2 shows each configuration with the amount of H_2 mass available according to maintain the weight of the aircraft for 1 and 2 passengers. the speed is the same. however, as will be seen below, the range and endurance are significantly modified between the two systems. The UAV type helicopter, i.e. without people and completely autonomous, has a speed value that is lower than the configurations with passengers because this configuration must have the greatest possible range for a characteristic mission related to surveillance, liaison, rescue, etc. Cruise speed values have been obtained by integration of design parameters using the flow chart in Fig. 1. Drag, aerodynamics, and power are included in the calculations. Standard rotorcraft performance estimation methods are used, such as the classic momentum theory or semiempirical correlations for the drag coefficient, as described in Appendix B.

2.2. Take-off and climb power

In relation to the take-off and climb of the helicopter, the values obtained (Tables 3 and 4) are reasonably suitable for the type of mission it has to perform in any of the configurations presented in this work. The parameters are described in Table 3. The climb values are related to the gradual change in air density as the vehicle gains

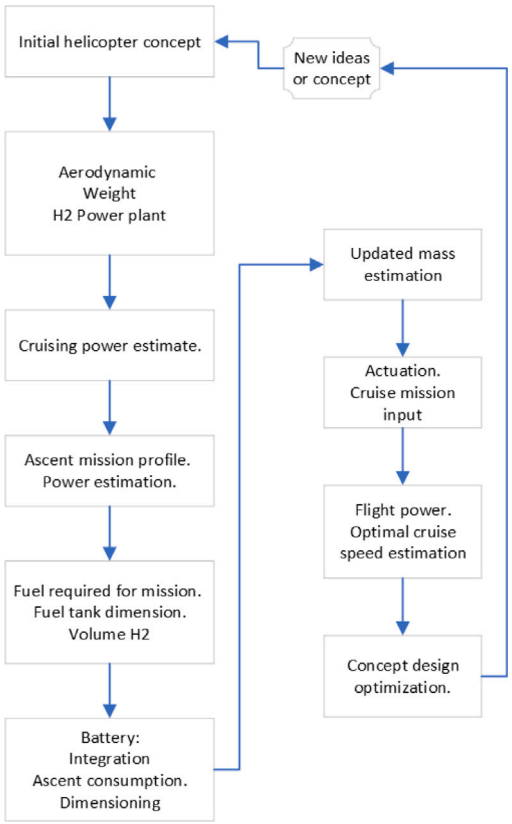

Fig. 1. Methods outline for the helicopter vehicle and propulsion system design.

Table 2
Performance data for the studied configurations.

Design	Pass.	Alt. [m]	Gross weight [kg]	P_{shaft} [kW]	Cruise speed [m/s]
1	0	0	416	51.4	135
		500	416	52.4	138
		1000	416	53.4	141
2	1	0	608	64.7	146
		500	608	65.9	149
		1000	608	67.3	153
2	0	0	533	53.6	137
		500	533	54.6	140
		1000	533	55.7	143
2	2	0	648	66,1	146
		500	648	67,2	149
		1000	648	68,3	153

altitude. Therefore, the analysis details that the fuel cell is sensitive to density changes. Maintaining a constant and efficient lift depends on the installed power as a function of altitude and must be aided by an auxiliary system to compensate for the density loss. In this work, as will be seen in Section 3, this is solved by imposing a battery that helps to maintain power and power distribution over the main and tail rotor.

In each of the tables, the average power to the axis has been calculated as the average of the powers generated by the rotor (data generated every 10 m) such that the helicopter can climb at the desired speed and taking into account losses of 5% in the DC–DC converter and the battery. In addition, the maximum power that can be supplied by the hydrogen FC has been estimated as the power of the H_2 cell (120 kW), taking into account the global losses in its operation (20%). Therefore a value of 96 kW is obtained. The figure is used for comparison when the power required by the axle at a certain height exceeds this value. This fact is important to take into account in this type of vehicles with a battery-based propulsion plant because according to temperature and density variations, there must be a power surplus which is represented by the battery. Consequently, the battery energy will be the integral of the difference between the average axle power minus the maximum deliverable power, taking into account that if the latter is higher there is no need to take into account this segment and taking into account another 10% of extra losses at the output of the battery. In the fifth column, the time during which the FCS is not enough to supply the power required for climbing is shown for each climbing velocity. The percentage in these cells represents the fraction of the time during the climb in which the battery is required to supply additional power. In the cases considered in this study, the battery is necessary always during climb for design 2 and its consumption is lower than its capacity, which is the result of the right sizing, but it could be possible that for lower climb rates the battery is only active at high altitude when the FCS maximum power output decays. For design 1, despite not using the battery for the climb operation, it is preserved with the same capacity since it is low and a battery is always required in these vehicles for the start of the FCS, to cover the electrical power demand of the components of the balance of plant during short and abrupt accelerations and in case of emergencies, such as the failure of the fuel cell. Despite these off-design situations not being modeled in the present study, the authors decided not to remove the battery even though it is not used during the ascend for design 1, since it provides an additional degree of redundancy, which is important to ensure safety in aerospace applications.

3. Methods on the hydrogen fuel cell propulsion system

In this section, a detailed description of the considered propulsion system and how it was optimized is provided. The optimization of the energy balance of the propulsion system was achieved through the development and validation of fuel cell system (FCS) numerical models (Section 3.1) whose balance of plant (BoP) management was adjusted to maximize the net FCS efficiency at different altitudes (Section 3.3).

The propulsion system proposed for the helicopter is based on H_2 FC technology, mainly due to the higher endurance and range that the usage of H_2 can provide, compared to batteries. In this sense, the specific energy of H_2 tanks together with the specific power of FC systems (FCS) implies that, for the same power demand and energy capacity, FC-based propulsion systems can offer lower weight and higher range/endurance, thus being more suitable for aerospace applications in which the volume and weight of the systems are critical.

The propulsion system is composed of a FCS to provide most of the power for the in-flight operations and cruise, a H_2 tank to store most of the energy to power the propulsion system, a small battery to provide additional power for the helicopter take-off, climb and in-flight performances, if required, and two electric motors to power the main and the auxiliary propellers. The sizing of each component is based on the results provided in Section 2 about the net power requirements to operate in cruise conditions (FCS and electric motors power), its consumption to provide a range of 300 km (H_2 tank capacity), and the additional power for take-off and climb (battery capacity).

The weight segmentation was based on data from the literature and the industry. FCS weight was calculated based on 2020 target of the DOE [28] for the specific power of FCS (0.65 kW_{net}/kg). Gravimmetric capacity of the liquid hydrogen tanks was based on the latest concepts for commuter aircraft [29] (0.2 kg H_2/kg syst.). Battery weight was estimated based on data from the industry [30] considering a battery system specific energy of 0.22 kWh/kg. Finally, the weight of the electric motors was obtained based on the specific power of the electric motor installed in the Toyota Prius HEV [31] (1.63 kW/kg).

Table 3
Required climb parameters in UAV configuration for design 1 (416 kg).

V_Z [m/s]	Alt. [m]	Average P_{shaft} in the ascent interval [kW]	Average P_{FCS} in the ascent interval [kW]	Time during which the FCS is not sufficient to supply climbing power [s]	Battery energy consumption [kWh]
5	500	54.3	60.0	0 (0%)	0
	1000	54.7	60.5	0 (0%)	0
6	500	56.7	62.7	0 (0%)	0
	1000	57.2	63.2	0 (0%)	0
7	500	59.2	65.4	0 (0%)	0
	1000	59.6	65.8	0 (0%)	0

Table 4
Required climb parameters in transport configuration for design 2 (608 kg).

V_Z [m/s]	Alt. [m]	Average P_{shaft} in the ascent interval [kW]	Average P_{FCS} in the ascent interval [kW]	Time during which the FCS is not sufficient to supply climbing power [s]	Battery energy consumption [kWh]
5	500	88.7	96.8	100 (100%)	0.03
	1000	89.5	96.3	200 (100%)	0.13
6	500	92.4	96.8	83.3 (100%)	0.12
	1000	93.2	96.3	166.7 (100%)	0.30
7	500	96.0	96.8	71.4 (100%)	0.20
	1000	96.8	96.3	142.9 (100%)	0.47

3.1. Fuel cell system model

The FCS model was developed using GT-Suite v2020 as the simulation and optimization platform. GT-Suite is a 0D-1D commercial modeling software widely used in the transport industry, particularly in the automotive sector, to perform simulations to solve fluid-dynamic, mechanical and electrical phenomena describing the operation of the components of any propulsion system. These phenomena are described by solving the continuity, momentum, energy and species conservation equations including the corresponding source terms when chemical or electrochemical reactions take place, together with extensively-used semi-empirical correlations to model simpler phenomena.

In any FC-based propulsion system, the FCS is composed by the FC stack (electrochemical energy generator) and the BoP (auxiliary components required to manage the stack and feed it with air, H_2 and coolant). The model describing the FC stack is mainly based on the following set of equations describing the polarization curve:

$$V_{FC} = V_{OC} - V_{act} - V_{ohm} - V_{mt} \tag{1}$$

$$V_{OC} = \frac{-\Delta \overline{g}_f}{2F} \tag{2}$$

$$V_{act} = \begin{cases} \frac{R_{gas}T}{2F}\left(\frac{i}{i_0}\right) \\ \frac{R_{gas}T}{2\alpha F}\log\left(\frac{i}{i_0}\right) \end{cases} \tag{3}$$

$$V_{ohm} = R_{ohm}\ I \tag{4}$$

$$V_{mt} = -C\ \log\left(1 - \frac{i}{i_l}\right) \tag{5}$$

where α is the charge transfer coefficient, C is the mass transport loss coefficient, F is Faraday's constant, i is the current density, i_0 is the exchange current density, i_l is the limiting current density, I is the current, R_{gas} is the ideal gas constant, R_{ohm} is the membrane ionic resistance and T is the temperature.

This set of equations describe how the FC voltage (V_{FC}) changes with the open circuity voltage (V_{OC}) and the electrochemical losses associated to the electrochemical activation reactions (V_{act}), the internal ohmic resistance (V_{ohm}) and the mass transport issues at high current density (V_{mt}). The calibration of such model mainly consist of selecting the right value for α, C, i_0, i_l and R_{ohm} that makes the model approach experimental results. Note that the parameters i_0 and R_{ohm} were modeled following the models developed by Murschenhofer et al. [32] and Terada et al. [33], respectively. This allowed the numerical integration of the dependence of the R_{ohm} to the membrane water content, temperature and membrane properties as well as the dependence of the i_0 to the FC temperature, the oxygen partial pressure, the electrochemical activation energy and the electrode roughness.

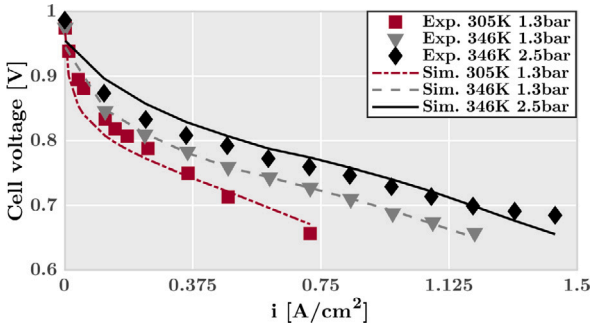

Fig. 2. Fuel cell model validation with experimental data from [34,35].

Unlike most of the studies that consider FC-based propulsion systems, the numerical model describing the FC stack behavior was validated at different conditions of pressure and temperature with the experimental data produced by Corbo et al. [34,35]. This is particularly critical for real operation in aerospace application since the inlet pressure of the propulsion system changes with altitude and the temperature is expected to be affected when the power output of the FCS changes. Therefore, in order ensure that the FC stack model has the right sensitivities to the expected operating conditions it was calibrated with empirical data obtained at different conditions of cathode pressure and stack temperature simultaneously (Fig. 2). For that purpose, genetic algorithms were used, resulting in an overall voltage error between the model and the experimental data of 2%. These polarization curves, given for a single cell, were used to scale up the FC stack to the power requirements of the UAV helicopter application (120 kW) by increasing the number of cells so that the target power output is produced close to the limiting current density.

Once the FC stack model was calibrated, it was integrated into a BoP, thus conforming a FCS. This FCS was developed in previous

studies and optimized for automotive applications [9,10]. A general sketch of all the components integrated in the FCS can be found in Fig. 3. These components can be classified as those belonging to the cathode circuit (airpath), the anode circuit (H_2 path) and coolant circuit. The cathode circuit consists of an electric supercharger, whose power is extracted form the overall energy produced by the FC stack, with a valve at the outlet of the circuit to regulate the air mass flow and pressure followed by a heat exchanger, to decrease the temperature of the compressed air, and a humidifier to increase the relative humidity at the inlet of the cathode. This last component is particularly significant since it is used to extract water from the outlet of the FC stack and introduce it at the cathode inlet to increase the membrane water content and decrease its ionic resistance, thus increasing its efficiency. The electric supercharger consists of the saled map of the FC compressor ROTREX EK10AA-PT54 matching the air flow requirements of the stack, given its number of cells. The anode circuit is composed of a H_2 tank connected to the FC stack and to an active recirculation anode loop through a valve to regulate the anode pressure. The pump is mainly used to control anode stoichiometry (Eq. (7)) and to recirculate the non-consumed H_2 back to the anode inlet since in the anode there is always H_2 excess (stoichiometry is higher than 1) to prevent the FC stack from suffering local starvation. The cooling circuit is that of a conventional FC vehicle (liquid cooling) integrating a radiator and a coolant management system (pump) since liquid cooling is recommended for high-power FC stacks in which the rejected heat is significant and needs to be evacuated through the cooling channels in between the cells of the stack. The management of the pressure-regulating valves in the anode and the cathode, the air compressor, the H_2 and coolant pumps is controlled through calibrated proportional–integral–derivative (PID) controllers. The aforementioned cathode and anode stoichiometries, which have significant effect over the FCS efficiency, are defined as in Eq. (7), where $\dot{m}$ denotes the mass flow rate of consumed or supplied O_2 or H_2:

$$\lambda_{\text{cath}} = \frac{\dot{m}_{O_2\ \text{consumed}}}{\dot{m}_{O_2\ \text{supplied}}} \tag{6}$$

$$\lambda_{\text{an}} = \frac{\dot{m}_{H_2\ \text{consumed}}}{\dot{m}_{H_2\ \text{supplied}}} \tag{7}$$

In order to optimize the energy balance of the FCS (Section 3.3), the most critical aspect to be improved in the BoP is the air management strategy [36]. This is particularly important in aerospace applications since the increase in altitude implies a decrease in the air pressure at the inlet of the FCS, thus requiring an active control of the BoP to adjust the air management strategy to the flight altitude. As such, the rest of the operating parameters have lower effect on the overall energy balance and are set to values specifically selected to ensure normal operation and preserve the FCS integrity:

- Anode stoichiometry was always kept close to 3 to avoid anode starvation that may lead to the FC stack malfunctioning or severe degradation.
- Anode pressure was kept 0.3 bar above cathode pressure to improve H_2 diffusion through the membrane. In this sense, a limit was imposed on the PID controlling the pressure of the anode circuit to preserve the FC stack integrity.
- The humidifier was set so that the cathode inlet relative humidity (RH) is kept, when possible, to 80% to ensure sufficient membrane humidity.
- Cathode inlet pressure was kept always over 1.2 bar to overcome the pressure loss in the FC stack and below 2.5 bar to preserve the mechanical integrity of the FC stack.

3.2. Propulsion system architecture

Fig. 4 shows an schematic of the propulsion system architecture integrating the FCS, a battery for additional power when the FCS cannot

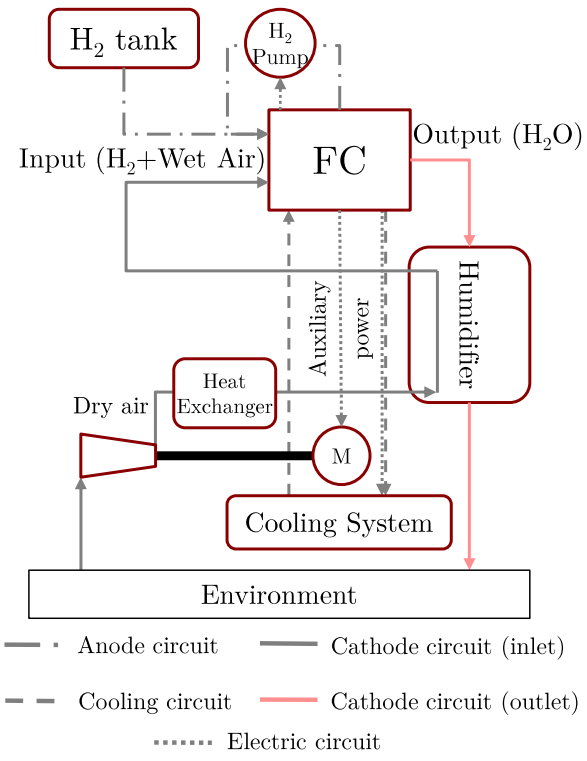

Fig. 3. Fuel cell system outline integrating the FC stack and the components of the BoP [9].

comply with the power demand from the rotor, and the electric motor. The electric architecture is indirect-type, which means that DC–DC converters (modeled with constant efficiency of 95%) are connecting the direct current (DC) bus to the FCS and the battery. This architecture is integrated into the last-generation FC vehicles (FCV) since the DC–DC booster connecting the FCS to the DC bus allows the downsizing of the FC stack, thus increasing the specific power of the propulsion system, and protects it from the voltage oscillations and electric instabilities that may come from the bus, thus increasing its durability.

The battery pack is modeled according to the simple equivalent circuit approach, taking into account state of charge (SOC)-dependent internal resistance and open-circuit voltage as in [10]. The battery consisted of a set of lithium cylindrical cells with a nominal voltage of 3.6 V and a nominal capacity of 3.35 Ah. The cells were distributed so that the battery could offer enough power. A lumped mass thermal model was used to ensure that no overheating was produced in the battery. The battery is mainly used as an auxiliary element of the propulsion system to provide the additional energy required by the electric motor when it exceeds the FCS maximum power, as can be seen in Fig. 9 when, for a given climb rate, the FCS power demand is over the FCS maximum power. In this situation, the excess power is provided by the battery. Further information about the battery discharge rate or C-rate is provided in Section 4. The size of the battery does not have a significant impact on the range, provided that it has low weight, since it is mainly used for auxiliary power during the climb.

The electric motor map was based on the Toyota Prius electric motor [31] and scaled accordingly with the power and torque demands of the main and auxiliary electric motors (Fig. 5). In this sense, the e-motor map used for the main rotor was scaled to 80 kW and 100 kW for design 1 and 2 respectively (Tables 3 and 4) based on the maximum power demand for a climb velocity of 7 m/s at 1000 m (over the target of 6 m/s) by ensuring a power excess of >5 kW for emergency operation (Fig. 9) while the e-motor used for the auxiliary rotor was sized by considering 5% of the power of the main rotor.

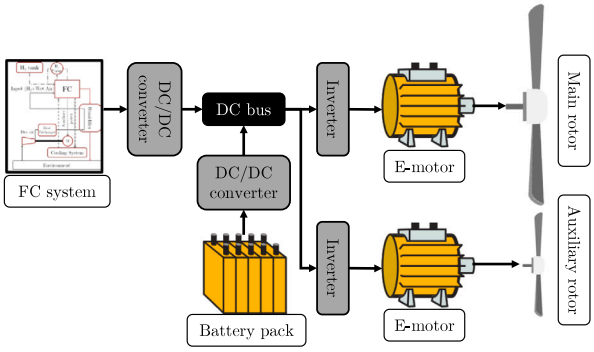

Fig. 4. Powerplant components outline, indirect-type FCV architecture.

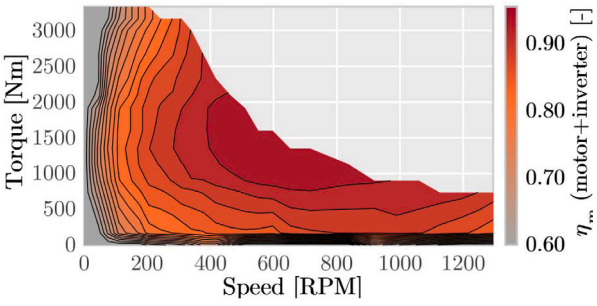

Fig. 5. Baseline electric motor+inverter map scaled from the Toyota Prius e-motor map [31].

3.3. Energy balance optimization

As commented in Section 3.1, the energy balance optimization consisted of finding the air management strategy that minimizes the air compressor consumption and the FC electrochemical losses, which is translated into maximizing the FC system net power output for a given current density. In this sense, a set of simulations by varying the cathode stoichiometry and compressor pressure ratio were carried out at sea level (SL), 500 m and 1000 m by varying the pressure and temperature environmental conditions according to the International Standard Atmosphere (ISA) model [37]. These altitudes were selected since SL is representative of the take-off condition, 500 m is the cruise altitude and 1000 m is closer to the usual maximum altitude at which the helicopters operate. Note that the energy balance optimization is performed at different altitudes independently since the environmental conditions affect significantly the electrochemical losses of the FC stack and thus the air management strategy should be aware of the change in the boundary conditions to minimize the power loss of the powerplant with altitude. As a consequence, the results given in this study should represent the evolution minimum power loss and maximum efficiency with altitude of this particular FCS.

Fig. 6 shows the compressor operating conditions that maximize the FCS efficiency given a current density. As can be seen, the higher the current density the higher the corrected mass flow rate for a fixed altitude since the current density is proportional to the flow of electrons through the membrane, hence proportional to the H_2 and O_2 consumption as well. Nonetheless, for current densities lower than 0.2 A/cm^2 the mass flow rate remains fixed at a minimum value to prevent the compressor from going into surge conditions. This implies that for $i < 0.2$ A/cm^2 the amount of air introduced in the cathode is significantly higher to that required FC stack, i.e., the cathode stoichiometry (Eq. (6)) will be significantly bigger than 1. For higher values of current

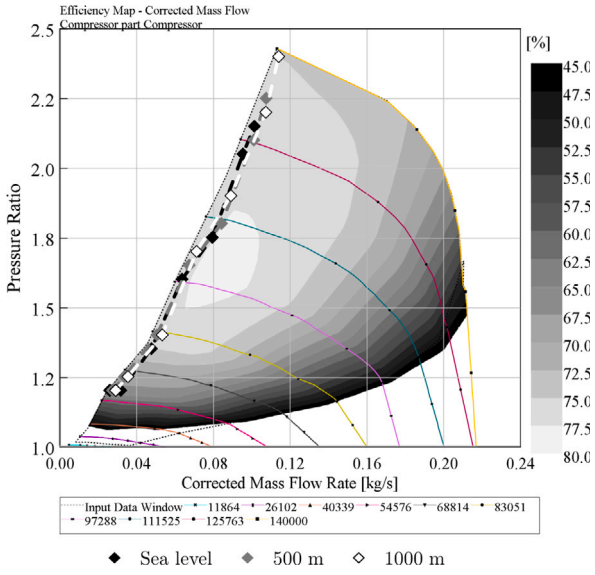

Fig. 6. Optimized air management strategy represented on the FCS compressor map for different altitudes.

density, the optimum operation is reached at the minimum cathode stoichiometry (imposed at 1.7–1.8 to avoid local cathode starvation, which may lead to FC degradation and malfunctioning). This means that minimizing the air mass flow rate maximizes the FCS efficiency since the decrease in FC electrochemical losses when increasing the cathode stoichiometry is outweighed by the increase in the air compressor power consumption (almost proportional to air mass flow rate). In contrast, the optimum compressor operation in Fig. 6 suggests that, for each value of corrected mass flow rate, the pressure ratio should be maximized to increase the FCS efficiency. As such, contrary to mass flow rate, increasing the cathode pressure decreases the FC losses more than the subsequent increase in the consumption of the air compressor. Note that this implies that, for extremely dynamic operation, care should be taken to prevent the compressor from entering into surge condition since the optimum operation is close to the surge line.

Changing the altitude by imposing the FCS inlet pressure and temperature according to the ISA model implies that, for the same cathode mass flow rate (cathode stoichiometry), the air corrected mass flow rate increases. Despite this, the trend of maximizing the compressor pressure ratio for a given mass flow is still perceived at 500 m and 1000 m. This behavior is shown in Fig. 6 sine the points showing the optimum compressor operation are displaced towards the right side of the map (to preserve the imposed value of cathode stoichiometry) and the upwards to increase the pressure ratio and thus maximize the FCS efficiency. Note that for 1000 m the corrected mass flow rate at maximum current density (1.3 A/cm^2) coincides with the point in the map with maximum pressure ratio. In case of going to higher altitudes this point would be displaced towards the right-hand side of the map, which irremediably implies lower maximum compressor ration. This implies that the rate of decay of the FCS maximum power output and efficiency with altitude may be increased for this particular FCS from 1000 m.

The resulting optimum FCS energy balance at different altitudes with the optimum air management strategy is shown in Fig. 7. This graph shows the fraction of the total energy introduced into the FC stack, computed as the H_2 times its lower heating value, that is produced as electrical FCS net power (red), consumed by the air compressor (black), the H_2 pump (blue) or the coolant pump (orange), and lost due to electrochemical inefficiencies (violet). Note that this way of showing the FCS energy balance is useful to identify both the FC stack and FC system efficiencies. The value given by the red bar, representing

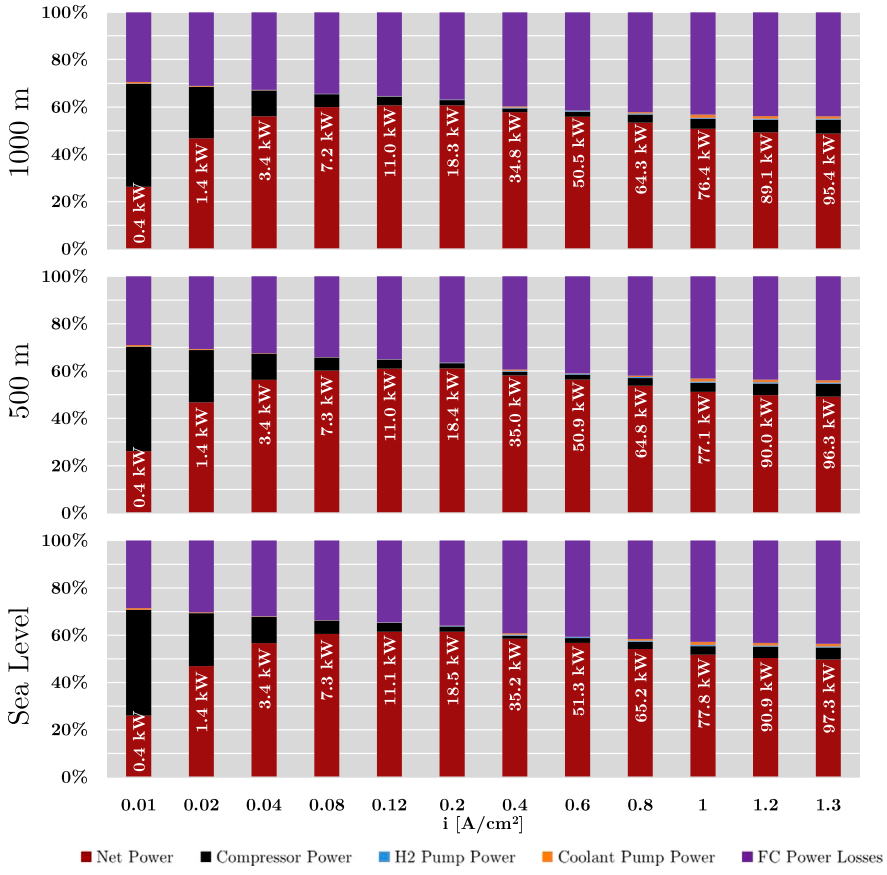

Fig. 7. Optimum FC system energy balance distribution with altitude for the FCS of design 2 (120 kW of FC stack maximum power).

Table 5
Results of the calculation process for PEMFC-helicopter concept for design 1 and design 2 (with all the variations) for cruise conditions at different altitudes.

Design	Pass.	Alt. [m]	Weight [kg]	P_{shaft} [kW]	P_{FCS} [kW]	Specific Range [km/kg]	Specific Endurance [km/kg]	H_2 mass [kg]
	0	0	416	39.6	46.9	47.8	21.3	6.5
1	0	500	416	40.5	47.8	47.1	20.8	6.5
	0	1000	416	42.0	50.2	46.2	20.4	6.5
	1	0	608	64.7	75.2	33.8	13.9	9.0
2	1	500	608	67.0	77.9	33.5	13.1	9.0
	1	1000	608	68.8	80.0	33.3	12.5	9.0
	0	0	533	54.7	64.3	40.4	16.9	9.0
2	0	500	533	55.7	65.3	40.2	16.4	9.0
	0	1000	533	57.7	67.6	39.2	15.5	9.0
	2	0	648	65.7	77.2	33.5	14	1.0
2	2	500	648	68.0	80	32.9	14.2	1.0
	2	1000	648	69.5	81.0	32.4	14.6	1.0

the FCS net power, is also the FCS net efficiency while the sum of the FCS net power, air compressor, H_2 pump, and coolant pump power represents the total power produced by the FC stack and the FC stack efficiency. For that reason, the evolution of the FCS net power with the current density in this graph is actually the FCS power curve while the evolution of FC stack power (net power and auxiliaries) represents the FC efficiency curve, which is the polarization curve if multiplied by the ideal open circuit FC voltage.

Following this optimization strategy that adapts the air compressor management according to the FC stack current density and the altitude, it is possible to identify the potential of FC-based powerplants for aerospace applications. As can be seen in Fig. 7, the maximum net power that the FC system can produce is 97.3 kW with a FCS efficiency of 49.7% at a current density of 1.3 A/cm^2. These values drop to 96.3 kW and 49.2% at 500 m and to 95.4 kW and 48.7% at 1000 m, respectively. This implies a power and efficiency loss of 2% when comparing the FCS performance at sea level and at 1000 m. Such

a small power loss implies that the operational space of the vehicle is broader than that of a naturally-aspirated reciprocating internal combustion engine (ICE), which losses roughly 3% of total power capacity each 1000 ft, and similar to that of a turbocharged ICE, which does not loss any power until the critical altitude is reached if the turbocharger is selected correctly. Given the altitude range in this study, the data produced is not enough to make a fair comparison about the FCS power loss against the power loss of a turbocharged ICE since it would be required to simulate the optimization at altitudes bigger than the critical altitude for the ICE to understand if there is any benefit in terms of the rate of power loss with altitude when comparing a FCS with turbocharged ICE. Further studies are required in this field to understand this and to explore higher pressure ratio compressors designed for FCS since they are not limited by the presence of knocking as gasoline ICE.

As can be seen in Fig. 7, the flat behavior of the power curve of the FCS (evolution of the red bars with the current density) does not change significantly. In this sense, the maximum FCS net efficiency is found at a current density of 0.2 A/cm^2 regardless of the altitude and has a value of 61.5%, 61.1% and 60.7% at sea level, 500 m and 1000 m respectively. This implies an efficiency loss at the maximum efficiency current density of 0.8% per 1000 m. Nonetheless, it is important to note that this trend may change slightly at higher altitude since in the optimization made at 1000 m showed a very close value of efficiency at 0.12 and 0.2 A/cm^2, which may imply that the value of current density providing the maximum FCS efficiency is displaced towards lower loads at higher altitudes for this particular FCS.

Finally, only with these results on this section, it is possible to conclude that the selected FCS with a FC stack of 120 kW may meet the power demands of propeller for the selected vehicle during cruise (Section 2.1), given that a certain amount of power will be lost in the DC–DC converter and in the e-motor+inverter (around 5% in each). As is seen in Section 4, the FCS has been oversized with respect to the power required for cruise to provide extra flexibility for climbing to downsize the battery pack and to decrease H_2 consumption. Oversizing the FCS is a common practice in the automotive sector since higher FCS maximum power implies that, for the same current density, the amount of power produced is higher. This also means that for a certain power demand, determined by the design and operating conditions of the vehicle, the FCS current density would decrease and its efficiency would increase, thus resulting in the decrease in H_2 consumption [9].

4. Results about the feasibility of a hydrogen fuel cell helicopter

As commented in Sections 2.1 and 2.2, the criteria for the sizing of the propulsion system was to achieve a range of at least 300 km at a cruise altitude of 500 m and a rate of climb of 6 m/s at 1000 m. As a result, the power that the FCS must supply was calculated by combining the in-flight calculation with the e-motor map (Fig. 5) and a 5% power loss in the DC–DC converter of the FCS. With these data, the FC stack power was set to 80 kW for design 1 and 120 kW for design 2 which implied a FCS maximum power varying between 63.6–64.9 kW and 95.4–97.3 kW respectively (Fig. 7). The FCS was slightly oversized as it was found that increasing its maximum power output made the FC stack operate under lower current densities, thus increasing the FCS efficiency. This, together with the evolution of the FCS efficiency with altitude and current density relating the H_2 consumption with the FCS power output (Fig. 7), the total mass required for the 300 km of range was calculated. Note that although the calculation process may seem direct, all these steps were integrated into the iterative process described in Fig. 1. Further from the helicopter operational targets, the constraint of 80 and 120 kW of FC stack power was imposed after the converged helicopter design and recalculated to improve the propulsion system efficiency since the preliminary sizing assumed a constant FCS efficiency of 50%. The final designs and performance parameters of each design can be found in Table 5. Note that all the data referred to design number 2 have the same propulsion system and vehicle architecture but they are used for different purposes. Design 2 was initially developed to carry 1 passenger with 20 kg of payload at 500 m with a range of 300 km (Table 1). In this sense, in order to explore the possibility of using this design in UAV mode (0 passengers) or with 2 passengers the mass distribution was changed. As can be seen in Table 1, in order to adapt design 2 to UAV mode, the H_2 tank and the payload weight were left untouched while the weight associated with the passenger was removed. This implied an increase in a specific range and endurance from 33.5 km/kg and 13.1 min/kg to 40.2 km/kg and 16.4 min/kg, respectively, which in absolute terms means an increase in range and endurance from 301 km and 118 min to 361 km and 147 min (+20% and +26% increase in range and endurance, respectively). Although the total range and endurance of design 2 with 0 passengers exceed the capabilities of design 1 (UAV) the use of H_2 is more efficient in design 1 since it was designed for a range of 300 km with a lower mass, which implies a lower power demand and thus lower H_2 consumption. This is reflected in the higher specific range and endurance of design 1.

In contrast, design 2 was adapted to carry 2 passengers (additional passenger of 75 kg) by removing the payload weight and decreasing the H_2 tank mass by keeping constant the total vehicle mass. As a consequence, the mass of H_2 stored in the tank was decreased from 9.0 to 1.0 kg while the specific range and endurance were kept constant since they only depend on the propulsion system efficiency which remains constant for a fixed vehicle mass. Therefore, the absolute values of range and endurance decreased from 301 km and 118 min to 34 km and 13 min, which may be high enough for aerotaxi application (urban transport) since the flight speed at 500 m for this design is 155 km/h. For longer range and endurance, the H_2 mass in the tank could be increased but the calculation process should be re-done. Note that the use of low-capacity tanks also implies a decrease in the refilling time, which may be beneficial in terms of actual vehicle utilization.

In terms of the actual distance to be covered during a mission, this means that both design 1 and design 2 with 0 and 1 passengers could go from the center of a country such as Spain to almost any part of its territory with just a single fill. Fig. 8 shows an application example of the mission range that the designed vehicles could achieve over the map of an actual country such as Spain from its capital, provided that the mission is one-way without refilling. This shows how the concept arising from the combination of FCS and helicopter technologies, in all of its variations, could achieve an acceptable range for missions such as the transport of any emergency good (for example organ transport) from the center of a country such as Spain to almost any part of its territory (see black and white shaded mission radius in Fig. 8). Furthermore, the range of 34 km provided by design 2 with 2 passengers (aerotaxi application) seems high enough for urban transport since it covers the whole surface of a big city such as Madrid, and could be even used for 2–3 displacements before requiring a refill.

As seen in Table 5, the power required by the FCS for cruise is well below the maximum power that the FCS can provide (63.6–64.9 kW for design 1 and 95.4–97.3 kW for design 2), which implies that for each of the designs proposed, the maximum reachable altitude is over 1000 m. By design imposition, the range of designs 1 and 2 (with 1 passenger) is 300 km at 500 m, but this range only decreases only by 0.1–1.8% at 1000 m, which implies that the operability and capabilities in terms of range and endurance of this vehicle remain almost unchanged in all the operation space. This little decrease is both due to the small increase in shaft power to sustain cruise conditions and to the prior optimization of the FCS efficiency at each altitude and current density.

For both designs 1 and 2, given the sizing of the FCS exceeding the power requirements for cruise in most of the operating conditions and the requirement for a battery to provide additional power in case of emergency or peak power demands, the operation of the helicopter could be further optimized to minimize H_2 consumption if the profile of the mission is known by using part of the energy stored in the battery

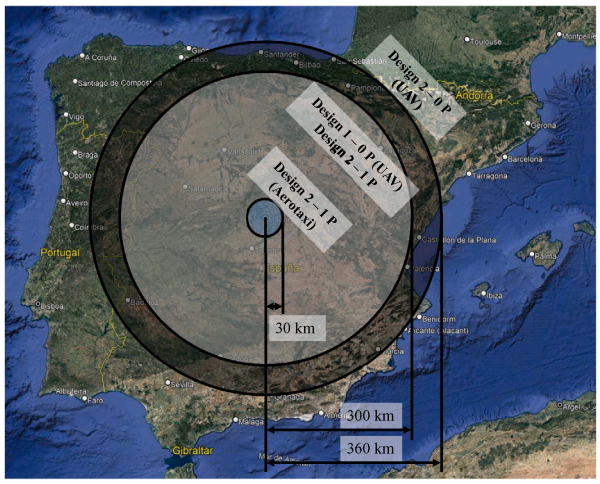

Fig. 8. Map of Spain illustrating the range of the different designs and variations of design 2 in Table 5.

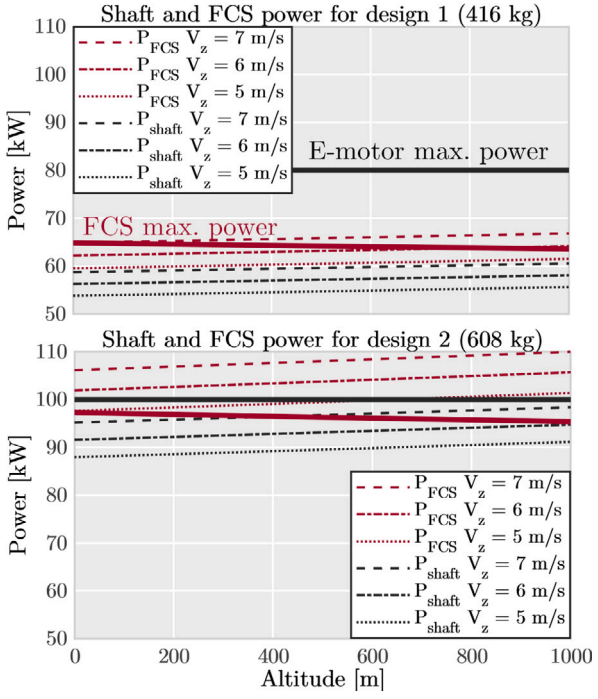

Fig. 9. Shaft and FCS power evolution with altitude at 5, 6 and 7 m/s climb speed for designs 1 and 2. The thick red line represents the evolution of the FCS maximum output power and the thick black line represents the e-motor maximum power.

to minimize the power provided by the FCS. Note that in this case the decrease in the state-of-charge of the battery, given a known missions profile, could be compensated by regenerating the power excess in the shaft when the helicopter descends, thus increasing not only the overall propulsion system efficiency but also the amount of energy the helicopter can make use of.

Regarding the requirements for climbing, as stated in Section 3.2, the electric motors were sized in such a way that a climb rate of 6 m/s at 1000 m was achievable with a margin of ~5 kW with respect to the maximum brake power (design 2). Fig. 9 shows the evolution of the shaft and FCS power required for baseline designs 1 and 2 for climbs rates of 5, 6 and 7 m/s together with the FCS maximum output power and the e-motor maximum brake power. In this graph, it is possible to understand that the FCS sizing has been performed to achieve the target cruise range and endurance but it requires a battery to provide a climb rate of 6 m/s at 1000 m in the most restrictive design (design 2 with 608 kg) while it can mostly climb at a rate of 6 m/s at 1000 m only with the FCS with design 1. In this sense, the FCS size was selected carefully not to impose extremely high battery discharge rates (C-rate) in the battery to achieve such as climb rate. Particular to design 2, for 6 m/s the average C-rate of the 2.4 kWh (considering an 80%–85% of usable energy) battery is 3 up to 500 m and 3.7 up to 1000 m, while it is 5.1 up to 500 m and 5.9 up to 1000 m for the 7 m/s rate of climb. The highest C-rate (5.9) implies that the battery energy would only last for around 10 min under this condition. Since this climb rate is to increase the altitude to 1000 m with a climb rate of 7 m/s, the time required for it would be around 2.5 min, which implies that the battery would consume less than half of its entire energy capacity for the most demanding climb condition. Note that the maximum rate of climb for this design is 7 m/s at 1000 m but it could be even higher at lower altitudes and can be close to 6 m/s even at 1500 m. This was motivated by the brake power output margin offered by the e-motor. The reader should note that the climb rate to reach such altitudes implies a very low climbing time (lower than 3 min to reach 1000 m at 6 m/s), which is translated in significantly low energy consumption from the battery, as can be seen in Table 4. This implies that there exists the possibility of using the vehicle to carry out several missions before recharging the battery or even utilizing it to decrease the H_2 consumption during cruise. In this sense, given the steady nature of the power demand evolution for this vehicle and the missions it is used to carry out, the durability of both the FCS and the battery may be enough during the lifetime of the vehicle.

In the case of design 1 (1st graph of Fig. 9) the installed FCS power is enough to cover the power requirement of the climb rate of 6 m/s, so the battery is only preserved in case of emergency, and to provide additional power for other power requirements arising from other systems other than the propulsion system such as all the electronic devices that may be included as part of the payload (design 1 is a pure UAV vehicle). The battery was not removed from the design since it may be used for two main purposes: to provide additional energy to heat up all the systems during a cold start in extreme conditions and to increase the overall efficiency of the propulsion system since during the descent part of the energy from the shaft could be regenerated by charging the battery. Furthermore, hybrid control strategies involving the use of the battery and the FCS in parallel during cruise may increase the range and endurance of the vehicle, thus providing an additional degree of freedom to further optimize the energy management strategy of the vehicle.

The helicopter concept in the single-passenger or one-pilot version is defined by Fig. 10, where it is described the dimensions of the tanks and the place they would be located with the hydrogen that has been calculated for this version and in accordance with the results obtained for the range or autonomy.

5. Potential for industry applications

The results obtained in this study are fully transferable to the industry since it provides insight about how the size of the components of the propulsion system and the aerodynamic design should be for an FC-powered light helicopter. Further from the target application of this study, the results in Section 3.3 help identify what is the potential power loss of a FC with altitude up to 1000 m if the air management strategy is altitude-aware. This is critical, not only for helicopter but also for low altitude fixed-wind aerial vehicles and for road transport applications. With the methods followed in this study, it would be possible to understand how the air management strategy should be adapted and it would help obtaining valuable data about the propulsion system operation to feed any energy management strategy controlled

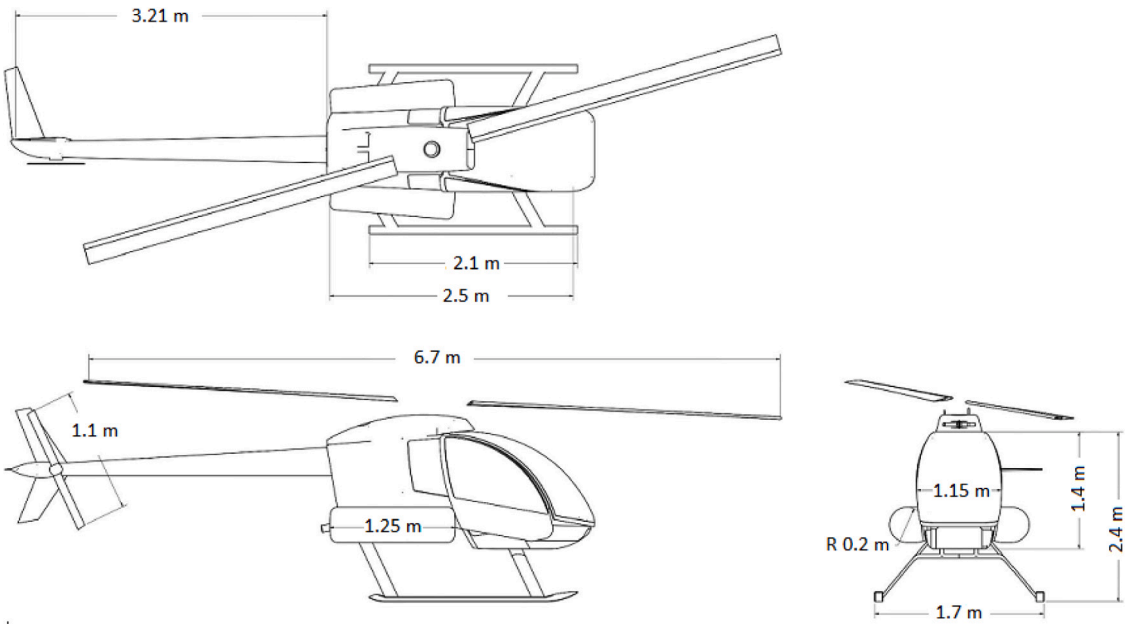

Fig. 10. Theoretical–conceptual design of the helicopter.

that ensures the optimum power split between the battery and the FC, thus minimizing the H_2 consumption and maximizing the vehicle range and endurance.

Nonetheless, the fact that these results are applicable in the short term to the industry depends on the development of high energy density and gravimetric capacity H_2 tanks. For the moment, the cost of such systems could be high enough that these vehicles only can make sense for specific missions and with funding from national or international entities. Nonetheless, this is to be expected since this is state-of-the-art technology that is not integrated into the transportation sector yet. Therefore, it is suggested that light helicopters powered by FC propulsion systems are developed and validated in captive fleets while the H_2 storage technology is further developed, as it was done with other transport applications such as FC-powered buses.

6. Conclusion

The paper presents a conventional rotary-wing vehicle in the light helicopter segment with a propulsion system based on hydrogen fuel cell technology and aimed at proving the feasibility of this concept that responds to the new missions in urban and interurban zero-emission mobility transport. For that purpose, a simulation platform integrating both the aerodynamic design and the propulsion system architecture was developed. The vehicle was calculated based on two different configurations using systems of linear equations integrated into the design development as shown in the flow chart in Fig. 1. The aerodynamic models were used to calculate the shaft power demands during cruise and climb through an iterative process based on the sizing of the components with a target range of 300 km at a cruise altitude of 500 m and a rate of climb of 6 m/s at 1000 m. The iterative process was based on combining the aerodynamic models together with the propulsion system models, consisting of a FCS, a small battery and an e-motor map model to obtain an accurate value for the overall efficiency of the propulsion system to estimate the right sizing of each component and the total mass of the vehicle. Then, the calculated mass and sizing of the components were introduced in the aerodynamics calculation to obtain a new value for the shaft power demand under cruise conditions. This iterative procedure was used until 2 designs were obtained: design 1 for UAV applications (0 passengers) and design 2 for aerotaxi applications (1 passenger with 20 kg of payload) as the baseline. Through the iterative process, the FC stack maximum power was fixed to 120 kW (over the power demand required by the vehicle) to allow the FCS operate under lower current densities to increase the efficiency of the propulsion system and provide extra power capacity for emergency situations. This decision was taken based on the FCS efficiency optimization performed in Section 3, on which a validated FC model was integrated into a BoP whose management was optimized at 0, 500, and 1000 m of altitude and current density ranging from 0.01 to 1.3 A/cm^2. Unlike most of the studies in the literature, the result of the FCS optimization at different altitudes provided not only the FCS efficiency evolution with the output power and the current density, but also the maximum power and efficiency decay due to the increase in altitude (from 97.3 kW to 95.4 kW and from 61.5% to 60.7%, respectively for the FCS of design 2) which indicated that the FCS technology, if optimized properly, is suitable for the helicopter application given the low power decay.

The converged iterative process provided a detailed mass segmentation (Table 1), flight requirement description for cruise (Table 2) and climb (Tables 3 and 4) conditions. From the baseline configuration of design 2 (for 1 passenger), this design was adapted to understand its change in range and endurance if the same propulsion system and vehicle were used for UAV application (0 passengers) and 2 passenger application. The results obtained in this study for cruise conditions show how the concept design for a helicopter for UAV, 1 and 2-passenger application is proven to be feasible in terms of energy flows and performance, achieving acceptable range, endurance and rates of climb for a wide range of altitudes (Table 5). In this sense, design 2 (developed initially to carry only 1 passenger and 18 kg of payload) could be adapted for UAV application to increase its range from 300 km to 360 km and for aerotaxi application to carry 2 passengers with range and endurance of 34 km and 13 min respectively. As such, these configurations offer relevant autonomy to fulfill a link between neuralgic points of any modern city, which is enough to meet the requirements of aerotaxi urban transport application.

Nomenclature

Abbreviations	
BoP	Balance of plant
C-rate	Discharge rate
DC	Direct current
FC	Fuel cell
FCS	Fuel cell system
FCV	Fuel cell vehicle
ICE	Internal combustion engine
ISA	International Standard Atmosphere
PID	Proportional–integral–derivative controller
RH	Relative humidity
SL	Sea level
SOC	State of charge
UAV	Unmanned air vehicle
VLR	Very light rotorcraft
Roman letters	
B	Blade tip correction factor
C	Mass transport loss coefficient
C_D	Drag coefficient
$C_{d,0}$	Average blade airfoil drag coefficient
$\Delta\bar{g}_f$	Gibbs free energy
F	Faraday's constant
f_z	Equivalent vertical cross section of the fuselage
I	Current
i	Current density
i_l	Limiting current density
i_0	Exchange current density
$\dot{m}$	Mass flow
P_0	Profile drag power losses
P_{cruise}	Cruise power
P_{FCS}	Fuel cell system power output
P_{shaft}	Shaft power
R	Rotor radius
R_{gas}	Ideal gas constant
R_{ohm}	Membrane ionic resistance
S	Rotor disk area
T	Temperature, thrust
V	Airspeed
V_{act}	Electrochemical activation losses
V_{FC}	Fuel cell voltage
V_{mt}	Mass transport at high current density losses
V_{ohm}	Internal ohmic resistance losses
V_{OC}	Open circuit voltage
V_z	Ascent speed
v_i	Induced speed
$v_{i,0}$	Induced speed in hover
W	Vehicle weight
Greek letters	
α	Charge transfer coefficient, angle of attack
κ	Compressibility correction factor
λ	Induced inflow ratio
λ_0	Induced inflow ratio in hover
λ_{an}	Anode efficiency
λ_{cath}	Cathode efficiency
μ	Advance ratio
Ω	Rotor rotational speed
σ	Blade solidity
ρ	Air density

CRediT authorship contribution statement

A. Tiseira: Conceptualization, Supervision, Formal analysis, Resources, Methodology, Writing – original draft. **R. Novella:** Formal analysis, Supervision, Project administration. **L.M. Garcia-Cuevas:** Resources, Data curation, Writing – review & editing. **M. Lopez-Juarez:** Investigation, Methodology, Validation, Software, Writing – original draft.

Data availability

Data will be made available on request.

Acknowledgments

This research has been partially funded by the Spanish Ministry of Science, Innovation, and University through the University Faculty Training (FPU) program (FPU19/00550) and FEDER and the Generalitat Valenciana, Consellería d'Innovació, Universitats, Ciencia i Societat Digital through project IDIFEDER/2021/039. Funding for open access charge: CRUE-Universitat Politècnica de València.

Appendix A. Similar aircraft data

Table A.6 contains the payload, operating empty mass, maximum takeoff mass, cruise power and takeoff power of 9 very light rotorcraft that have been used for sizing the vehicle described in this work. Table A.7, in the other hand, shows size data such as the fuselage length L_{fuselage}, the cabin width w_{cabin}, the helicopter height h, the total length L_{total}, the main rotor diameter D_{main} and the tail rotor diameter D_{tail}. Finally, Table A.8 shows their endurance, range cruise speed V_{cruise}, climb speed V_z and main rotor rotational speed n_{main}. All these helicopters fly with one pilot and one passenger and all but the Sython AH 130 are powered by a reciprocating internal combustion engine, which uses a small turboshaft.

Appendix B. Aerodynamic performance model of the vehicle

The aerodynamic performance model of the vehicle is computed using standard methods, as described in classic aeronautical design and aerodynamics books such as 'Principles of Helicopter Aerodynamics', by Leishman [38].

The cruise power P_{cruise} is computed as in Eq. (B.1) and makes use of the blade profile power losses P_0, defined in Eq. (B.2):

$$P_{\text{cruise}} = \frac{\kappa}{B} T v_{i,0} \frac{\lambda}{\lambda_0} + P_0 + \frac{1}{2}\rho V^3 C_D S \tag{B.1}$$

$$P_0 = \rho S (\Omega R)^3 \left(\frac{C_{d,0}\sigma}{8}\right)\left(1 + 3\mu + \frac{3}{8}\mu^4\right) \tag{B.2}$$

where κ is a correction factor due to compressibility effects and is approximated as 1.15, B is a correction due to tip losses, T is the rotor thrust, $v_{i,0}$ is the induced velocity in hovering conditions, λ is the induced inflow ratio, λ_0 is the induced inflow ratio for hovering conditions, ρ is the air density, S is the rotor disk area, Ω is the rotor rotational speed, R is the rotor radius, $C_{d,0}$ is the average drag coefficient of the airfoils of the rotor blades, σ is the blade solidity, μ is the advance ratio, V is the airspeed and C_D is the drag coefficient of the vehicle (referenced to the area of the rotor disk).

With no accelerations, the vertical component of the thrust T is equal to the weight of the vehicle W and the horizontal component is equal to the parasitic drag, $0.5\rho V^2 C_D S$.

The induced velocity in hover, $v_{i,0}$, is equal to $\sqrt{T/(2\rho S)}$, according to the classic momentum theory.

The advance ratio μ is defined as $V\cos\alpha/(\Omega R)$, being α the angle between the rotor axis and the airspeed.

The induced inflow ratio λ is defined as $\left(V\sin\alpha + v_i\right)/(\Omega R)$.

The blade solidity σ is defined as the actual blade platform area divided by the disk area.

The drag coefficient C_D is approximated by semiempirical correlations for all the vehicle elements, including the correction factors due

Table A.6
Similar aircraft data — mass and power.

Name	Payload [kg]	OEM [kg]	MTOM [kg]	P_{cruise} [kW]	$P_{takeoff}$ [kW]
Dynali H3	210	285	500	75.0	82.0
Dynali H2s	200	465	700	123.0	134.2
CH-7 Kompress	170	245	450	73.0	84.6
LC LH 212 Delta	123	280	450	73.0	84.0
RotorWay Exec 162F	193	442	680	89.6	112.0
RotorWay A600	204	441	680	87.7	109.6
Sython AH 130	225	290	580	97.0	111.6
Masquito M80		230	450	71.6	89.5
Dragon 34 GP		282	450	74.0	84.6

Table A.7
Similar aircraft data — sizes.

Name	$L_{fuselage}$ [m]	w_{cabin} [m]	h [m]	L_{total} [m]	D_{main} [m]	D_{tail} [m]
Dynali H3	6.00	1.30	2.50	7.80	7.14	0.80
Dynali H2s	6.23	1.45		7.95	7.22	0.80
CH-7 Kompress	5.31	0.82	2.31	7.41	6.27	1.03
LC LH 212 Delta	6.18	1.27	2.35	7.92	6.75	1.20
RotorWay Exec 162F	6.70	2.40	680	9.00	7.62	1.20
RotorWay A600	6.70	1.10	2.60	9.00	7.90	1.20
Sython AH 130			2.40	8.84	7.63	
Masquito M80	4.85	1.30	2.25	6.22	5.52	1.00
Dragon 34 GP	5.56	1.15	2.36	7.86	6.60	1.12

Table A.8
Similar aircraft data — range, endurance and speeds.

Name	Endurance [h]	Range [km]	V_{cruise} [m s^{-1}]	V_z [m s^{-1}]	n_{main} [rpm]
Dynali H3	2.50	350	38.89	4.60	515–565
Dynali H2s	3.15	550	45.83	6.60	530
CH-7 Kompress	3.75	552	44.44	7.50	520
LC LH 212 Delta	3.00	495	45.83	8.50	
RotorWay Exec 162F	2.00	290	42.50	5.10	
RotorWay A600	2.00	290	40.23	4.06	
Sython AH 130	1.50	275	51.39	8.50	
Masquito M80	4.00	600	41.11	5.59	690
Dragon 34 GP	2.00	300	33.33	6.50	520

to aerodynamic interference between elements. The value of $C_{d,0}$ is also approximated from typical values of rotor blades.

The ascending power P_{asc} is computed as in Eq. (B.3).

$$P_{asc} = \frac{W}{1 - f_z/S}\left[\frac{V_z}{2} + \sqrt{\frac{W}{2\rho S\left(1 - f_z/S\right)}}\right] + P_0 \tag{B.3}$$

where W is the helicopter weight, S is the disk area, V_z is the ascent speed, ρ is the air density and f_v is the equivalent flat area for the vertical cross section of the fuselage, which is usually approximated as $0.05S$.

References

[1] ICAO Unitin Aviation. Effects of novel coronavirus (COVID-19) on civil aviation: Economic impact analysis. Econ Dev Air Transp Bureau 2022;1–116.

[2] Jackson PA. Jane's all the world's aircraft 2004–2005. 2004.

[3] European Union Aviation Safety Agency. Easy access rules for very light rotorcraft. 2023, URL https://www.easa.europa.eu/downloads/68046/en. [Last accessed 28 February 2023].

[4] European Comission. 2050 Long-term strategy. 2023, URL https://ec.europa.eu/clima/eu-action/climate-strategies-targets/2050-long-term-strategy_en. [Last accessed 28 February 2023].

[5] Desantes J, Molina S, Novella R, Lopez-Juarez M. Comparative global warming impact and NOX emissions of conventional and hydrogen automotive propulsion systems. Energy Convers Manage 2020;221(X):113137. http://dx.doi.org/10.1016/j.enconman.2020.113137.

[6] McKinsey & Company. Hydrogen-powered aviation. 2020, http://dx.doi.org/10.2843/766989.

[7] Fuel Cells and Hydrogen Joint Undertaking (FCH JU). Hydrogen Roadmap Europe - A sustainable pathway for the European energy transition, http://dx.doi.org/10.2843/249013.

[8] Zhao P, García A, Burton T. Initiation and propagation of curved reaction front in solids: Insights into solid combustion and battery thermal runaway. Combust Flame 2022;238:111951. http://dx.doi.org/10.1016/j.combustflame.2021.111951.

[9] Molina S, Novella R, Pla B, Lopez-Juarez M. Optimization and sizing of a fuel cell range extender vehicle for passenger car applications in driving cycle conditions. Appl Energy 2021;285(December 2020):116469. http://dx.doi.org/10.1016/j.apenergy.2021.116469.

[10] Desantes JM, Novella R, Pla B, Lopez-Juarez M. Impact of fuel cell range extender powertrain design on greenhouse gases and NOX emissions in automotive applications. Appl Energy 2021;302:117526. http://dx.doi.org/10.1016/j.apenergy.2021.117526.

[11] Desantes J, Novella R, Pla B, Lopez-Juarez M. Effect of dynamic and operational restrictions in the energy management strategy on fuel cell range extender electric vehicle performance and durability in driving conditions. Energy Convers Manage 2022;266(X):115821. http://dx.doi.org/10.1016/j.enconman.2022.115821.

[12] Rašić D, Katrašnik T. Multi-domain and multi-scale model of a fuel cell electric vehicle to predict the effect of the operating conditions and component sizing on fuel cell degradation. Energy Convers Manage 2022;268(February). http://dx.doi.org/10.1016/j.enconman.2022.116024.

[13] Philip N, Ghosh PC. A generic sizing methodology for thermal management system in fuel cell vehicles using pinch analysis. Energy Convers Manage 2022;269(June):116172. http://dx.doi.org/10.1016/j.enconman.2022.116172.

[14] Desantes J, Novella R, Pla B, Lopez-Juarez M. A modeling framework for predicting the effect of the operating conditions and component sizing on fuel cell degradation and performance for automotive applications. Appl Energy 2022;317:119137. http://dx.doi.org/10.1016/j.apenergy.2022.119137.

[15] Abbas M, Cho I, Kim J. Reliability-constrained optimal sizing and rechargeable battery selection for improved load distribution in a fuel-cell hybrid railway propulsion system. Energy Convers Manage 2019;196(July):1167–79. http://dx.doi.org/10.1016/j.enconman.2019.06.061.

[16] Haseltalab A, van Biert L, Sapra H, Mestemaker B, Negenborn RR. Component sizing and energy management for SOFC-based ship power systems. Energy Convers Manage 2021;245(August):114625. http://dx.doi.org/10.1016/j.enconman.2021.114625.

[17] Ji Z, Rokni MM, Qin J, Zhang S, Dong P. Energy and configuration management strategy for battery/fuel cell/jet engine hybrid propulsion and power systems on aircraft. Energy Convers Manage 2020;225(August):113393. http://dx.doi.org/10.1016/j.enconman.2020.113393.

[18] Oh TH. Conceptual design of small unmanned aerial vehicle with proton exchange membrane fuel cell system for long endurance mission. Energy Convers Manage 2018;176(July):349–56. http://dx.doi.org/10.1016/j.enconman.2018.09.036.

[19] Ozbek E, Yalin G, Karaoglan MU, Ekici S, Colpan CO, Karakoc TH. Architecture design and performance analysis of a hybrid hydrogen fuel cell system for unmanned aerial vehicle. Int J Hydrogen Energy 2021;46(30):16453–64. http://dx.doi.org/10.1016/j.ijhydene.2020.12.216.

[20] Çalışır D, Ekici S, Midilli A, Karakoc TH. Benchmarking environmental impacts of power groups used in a designed UAV: Hybrid hydrogen fuel cell system versus lithium-polymer battery drive system. Energy 2023;262:125543. http://dx.doi.org/10.1016/j.energy.2022.125543.

[21] Datta A, Johnson W. Powerplant design and performance analysis of a manned all-electric helicopter. J Propuls Power 2014;30:490–505. http://dx.doi.org/10.2514/1.B34843.

[22] Santos DF, Ferreira RB, Falcão D, Pinto A. Evaluation of a fuel cell system designed for unmanned aerial vehicles. Energy 2022;253:124099. http://dx.doi.org/10.1016/j.energy.2022.124099, URL https://www.sciencedirect.com/science/article/pii/S0360544222010027.

[23] Federal Aviation Administration. Helicopter flying handbook. FAA H-8083-21B, U.S. Department of Transportation; 2019, URL https://www.faa.gov/regulations_policies/handbooks_manuals/aviation/helicopter_flying_handbook.

[24] Astridge DG. Helicopter transmissions—design for safety and reliability. Proc Inst Mech Eng G 1989;203:123–38. http://dx.doi.org/10.1243/PIME_PROC_1989_203_063_01.

[25] Prouty RW. Helicopter performance, stability, and control. 1990.

[26] US Department of Transportation. Rotorcraft flying handbook. 2000.

[27] Rajendran S. Real-time dispatching of air taxis in metropolitan cities using a hybrid simulation goal programming algorithm, 178. 2021, http://dx.doi.org/10.1016/j.eswa.2021.115056.

[28] US Department Of Energy. DOE technical targets for fuel cell systems and stacks for transportation applications. 2015, URL https://www.energy.gov/eere/fuelcells/doe-technical-targets-fuel-cell-systems-and-stacks-transportation-applications.

[29] Clean Sky 2 JU and FCH2 JU. Hydrogen-powered aviation: A fact-based study of hydrogen technology, economics, and climate impact by 2050. Tech. rep. May, 2020, http://dx.doi.org/10.2843/766989.

[30] Löbberding H, Wessel S, Offermanns C, Kehrer M, Rother J, Heimes H, et al. From cell to battery system in BEVs: Analysis of system packing efficiency and cell types. World Electr Veh J 2020;11(4):1–15. http://dx.doi.org/10.3390/wevj11040077.

[31] Burress TA, Campbell SL, Coomer CL, Ayers CW, Wereszczak AA, Cunningham JP, et al. Evaluation of the 2010 toyota prius hybrid synergy drive system 2010 toyota prius hybrid synergy. Tech. rep. March, Tennessee: Oak Ridge National Laboratory; 2011.

[32] Murschenhofer D, Kuzdas D, Braun S, Jakubek S. A real-time capable quasi-2D proton exchange membrane fuel cell model. Energy Convers Manage 2018;162(January):159–75. http://dx.doi.org/10.1016/j.enconman.2018.02.028.

[33] Terada I, Nakagawa H. Polymer electrolyte fuel cell. Kobunshi 2008;57(7):498–501. http://dx.doi.org/10.1295/kobunshi.57.498.

[34] Corbo P, Migliardini F, Veneri O. Experimental analysis and management issues of a hydrogen fuel cell system for stationary and mobile application. Energy Convers Manage 2007;48(8):2365–74. http://dx.doi.org/10.1016/j.enconman.2007.03.009.

[35] Corbo P, Migliardini F, Veneri O. Experimental analysis of a 20 kWe PEM fuel cell system in dynamic conditions representative of automotive applications. Energy Convers Manage 2008;49(10):2688–97. http://dx.doi.org/10.1016/j.enconman.2008.04.001.

[36] Desantes JM, Novella R, Pla B, Lopez-Juarez M. Driving profile influence on fuel cell range extender vehicle performance and global warming impact. In: SIA Powertrain & electronics 2021 digital edition R-2021-04. 2021.

[37] Standard atmosphere, vol. 1975. Standard ISO 2533:1975, Geneva, Switzerland: International Organization for Standardization; 1975.

[38] Leishman J. Principles of helicopter aerodynamics. University Printing House, Cambridge CB2 8BS, United Kingdom: Cambridge University Press; 2016.